

# DiffusionFF: Face Forgery Detection via Diffusion-based Artifact Localization

Siran Peng<sup>1,2\*</sup>, Haoyuan Zhang<sup>2,1\*</sup>, Li Gao<sup>3</sup>, Tianshuo Zhang<sup>2,1</sup>, Bao Li<sup>1,2</sup>, Zhen Lei<sup>1,2,4,5†</sup>

<sup>1</sup>MAIS, Institute of Automation, Chinese Academy of Sciences

<sup>2</sup>School of Artificial Intelligence, University of Chinese Academy of Sciences

<sup>3</sup>China Mobile Financial Technology Co., Ltd.

<sup>4</sup>CAIR, HKISI, Chinese Academy of Sciences

<sup>5</sup>SCSE, the Faculty of Innovation Engineering, M.U.S.T

{pengsiran2023, zhanghaoyuan2023, libao2023, zhen.lei}@ia.ac.cn, tianshuo.zhang@nlpr.ia.ac.cn

\*Equal contribution. †Corresponding author.

## Abstract

The rapid evolution of deepfake generation techniques demands robust and accurate face forgery detection algorithms. While determining whether an image has been manipulated remains essential, the ability to precisely localize forgery artifacts has become increasingly important for improving model explainability and fostering user trust. To address this challenge, we propose DiffusionFF, a novel framework that enhances face forgery detection through diffusion-based artifact localization. Our method utilizes a denoising diffusion model to generate high-quality Structural Dissimilarity (DSSIM) maps, which effectively capture subtle traces of manipulation. These DSSIM maps are then fused with high-level semantic features extracted by a pretrained forgery detector, leading to significant improvements in detection accuracy. Extensive experiments on both cross-dataset and intra-dataset benchmarks demonstrate that DiffusionFF not only achieves superior detection performance but also offers precise and fine-grained artifact localization, highlighting its overall effectiveness.

## Introduction

The rapid advancement of deepfake generation techniques (Hsu, Tsai, and Wu 2022; Shiohara, Yang, and Taketomi 2023) has enabled the creation of forged facial content with highly convincing perceptual quality, posing serious threats to information integrity and public trust. In response, developing robust and accurate face forgery detection algorithms has become increasingly critical. However, beyond the binary classification task of detecting manipulations, there is a growing recognition of the need to precisely localize forgery artifacts. By pinpointing the manipulation traces within an image, artifact localization provides concrete evidence that supports the model’s decisions, thereby improving explainability and reinforcing user trust. As a result, recent research has increasingly focused on artifact localization, viewing it as a powerful tool to advance face forgery detection systems.

However, the precise localization of fine-grained forgery artifacts remains a significant challenge. Conventional mask-based methods (Kong et al. 2022; Zhao et al. 2023; Hu et al. 2024) are inherently coarse and often struggle to delineate manipulation traces with the required level of detail. In contrast, some researchers have explored the use of Structural Dissimilarity (DSSIM) maps (Wang et al. 2004), which offer pixel-level sensitivity and can reveal fa-

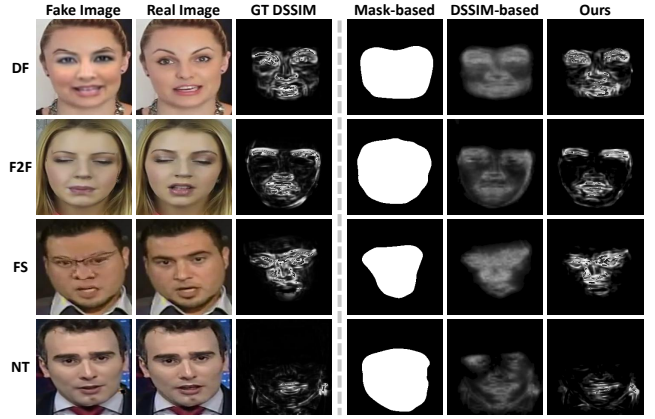


Figure 1: Visual comparison of the proposed DiffusionFF with mask-based and previous DSSIM-based localization methods across four manipulation types (DF, F2F, FS, and NT) from the FaceForensics++ (FF++) dataset (Rossler et al. 2019). The Ground-Truth (GT) DSSIM map is computed by comparing each fake image with its corresponding real image, using the algorithm detailed in the *Preliminaries* section. All models receive only the fake image as input.

cial forgery artifacts with greater granularity. Nevertheless, existing DSSIM-based approaches (Chen et al. 2021; Wang, Sun, and Tang 2022) are hindered by their reliance on direct regression frameworks, which tend to average out subtle inconsistencies, ultimately producing blurry localization maps that lack the desired fine-grained precision. A visual comparison of these methods is presented in Figure 1.

In (Wang, Sun, and Tang 2022), the generated DSSIM maps are incorporated into the network to enhance classification accuracy. Building on this idea, our experiments reveal a strong correlation between the quality of these maps and the resulting detection performance, as shown in Figure 2. Specifically, coarse DSSIM maps hinder the model’s ability to identify truly discriminative regions, leading to suboptimal results. In contrast, high-quality maps offer fine-grained and precise guidance, enabling more reliable explanations and substantial improvements in detection accuracy.

Considering these factors, we leverage the powerful gen-

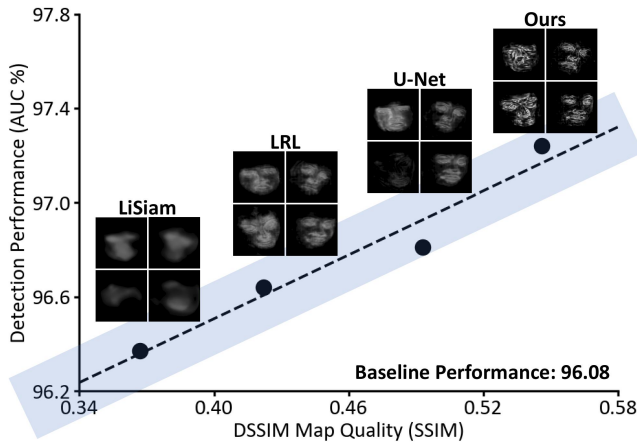


Figure 2: Correlation between DSSIM map quality and detection performance. We fuse the DSSIM maps generated by LiSiam (Wang, Sun, and Tang 2022), LRL (Chen et al. 2021), U-Net (Ronneberger, Fischer, and Brox 2015), and DiffusionFF with features extracted from a shared forgery detector to obtain the final classification results.

erative capabilities of denoising diffusion models (Ho, Jain, and Abbeel 2020) to create high-quality DSSIM maps, which enable precise artifact localization and significantly improve detection accuracy. Specifically, we propose DiffusionFF, a novel framework that enhances face forgery detection via diffusion-based artifact localization. Our method begins by utilizing a pretrained forgery detector to extract multi-resolution features from the input image. These forgery-related features then serve as guidance for a denoising diffusion model, which progressively generates a high-fidelity DSSIM map. Finally, this DSSIM map is fused with the detector’s output feature map to produce the classification result. The contributions of this paper are as follows:

- We introduce a novel approach that harnesses the powerful generative capabilities of denoising diffusion models to produce high-quality DSSIM maps, enabling precise and fine-grained localization of facial forgery artifacts.
- Our method integrates detailed DSSIM maps with high-level features extracted by a forgery detector, leading to substantial improvements in detection performance.
- The proposed DiffusionFF framework not only achieves state-of-the-art (SOTA) classification performance but also surpasses existing artifact localization methods in revealing manipulation traces, demonstrating its superior effectiveness, reliability, and explainability.

## Related Works & Motivation

### Face Forgery Detection

**Detection-only Methods.** Face forgery detection is commonly framed as a binary classification task. Existing studies, based on their underlying strategies, can be grouped into four main categories: spatial-domain, time-domain, frequency-domain, and data-driven approaches. Spatial-domain methods detect forgeries by examining image-level

artifacts such as color mismatches (He, Li, and Wang 2019), unnatural saturation (McCloskey and Albright 2019), and visual anomalies (Shiohara and Yamasaki 2022; Cui et al. 2025). Time-domain techniques model temporal dynamics across video frames to capture inter-frame inconsistencies (Yang et al. 2023; Zhang et al. 2024). Frequency-domain methods apply signal transforms like FFT (Tan et al. 2024), DCT (Qian et al. 2020), and DWT (Li et al. 2022; Miao et al. 2023) to expose subtle manipulation traces that are often imperceptible in the spatial or time domains. Lastly, data-driven approaches boost detection performance by leveraging advanced network architectures and optimized training strategies (Guo et al. 2023; Yan et al. 2024; Fu et al. 2025).

**Detection with Localization Methods.** In addition to detection-only methods, some studies have explored integrating artifact localization to enhance face forgery detection. These methods can be broadly classified into two types: mask-based and DSSIM-based approaches. Mask-based methods treat artifact localization as a segmentation task, generating binary masks that indicate forged regions. These methods primarily exploit semantic features, analyze noise patterns, or leverage meta-learning techniques to improve segmentation precision (Kong et al. 2022; Zhao et al. 2023; Hu et al. 2024). In contrast, DSSIM-based approaches aim to produce fine-grained, pixel-level localization maps that reveal subtle traces of manipulation. To improve localization quality, these approaches have employed attention mechanisms (Chen et al. 2021) or Siamese network architectures (Wang, Sun, and Tang 2022). Compared to coarse binary masks, DSSIM maps provide a more precise and detailed representation of facial forgery artifacts. However, existing DSSIM-based methods typically rely on direct regression frameworks, which tend to yield smooth and blurry outputs. This limitation hinders their ability to generate artifact localization maps with the desired fine-grained precision.

### Diffusion Models in Forgery Detection

In recent years, diffusion models (Ho, Jain, and Abbeel 2020) have emerged as a powerful class of generative tools, which iteratively transform noise into high-fidelity images by learning the underlying data distribution through a denoising process. In image forgery detection, DiffForensics (Yu et al. 2024) leverages diffusion models as robust image priors, effectively detecting manipulations and creating binary masks to highlight forged regions. However, utilizing such sophisticated models for generating coarse-grained binary masks might be seen as an overuse of their capabilities. In the specific area of face forgery detection, DiffusionFake (Chen et al. 2024) employs a Latent Diffusion Model (LDM) (Rombach et al. 2022) to reconstruct both the source and target identities from a single deepfake image. While this approach is innovative, it faces challenges in generalizing to unseen identities, which restricts its broader applicability.

### Motivation

Recently, researchers have increasingly explored incorporating artifact localization into face forgery detection systems to enhance both classification accuracy and model ex-

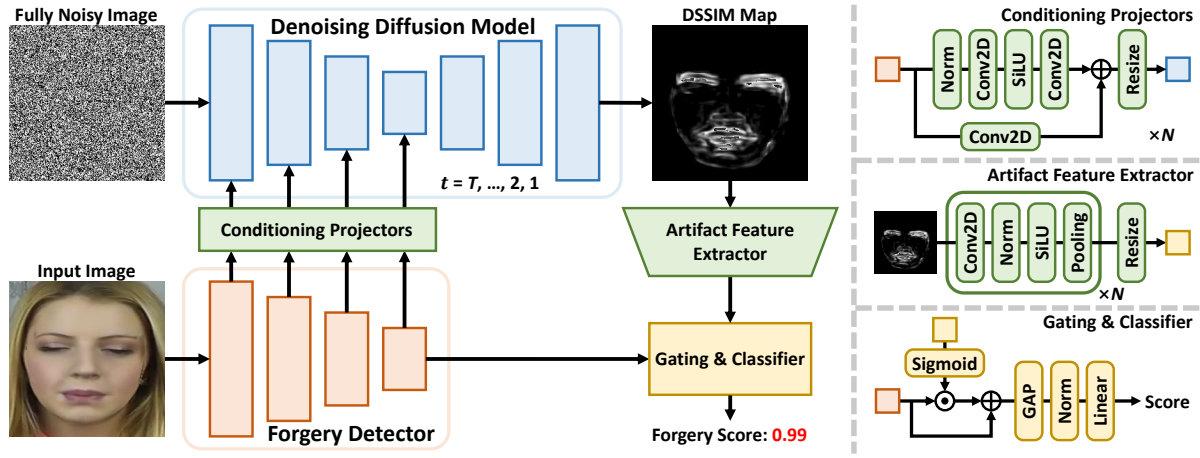


Figure 3: Overview of DiffusionFF.  $N$  is the number of stages in the detector, while “GAP” denotes Global Average Pooling.

plainability. Conventional mask-based methods tend to provide only coarse localization of forged regions. On the other hand, while DSSIM maps can capture fine-grained manipulation artifacts, DSSIM-based approaches often suffer from blurry outputs due to their dependence on direct regression frameworks. To overcome these challenges, we leverage denoising diffusion models to generate precise, detailed localization maps. Furthermore, by fusing these maps with high-level features from the forgery detector, our method demonstrates substantial improvements in detection performance.

## Methodology

### Preliminaries

**GT DSSIM Map Formulation.** To obtain Ground-Truth (GT) DSSIM maps that supervise the training of denoising diffusion models, we first extract frames and crop faces from both the original video and its manipulated counterparts, ensuring consistent settings across different video types. This process yields a set of fully aligned image pairs. For each image pair, we compute the DSSIM map by sliding a local window across the two images and calculating the DSSIM value at each pixel location  $(i, j)$ . The formula is given by:

$$\begin{aligned} \text{DSSIM}(i, j) &= 1 - \text{SSIM}(x, y), \\ \text{SSIM}(x, y) &= \frac{(2\mu_x\mu_y + C_1)(2\sigma_{xy} + C_2)}{(\mu_x^2 + \mu_y^2 + C_1)(\sigma_x^2 + \sigma_y^2 + C_2)}. \end{aligned} \quad (1)$$

Here,  $\text{DSSIM}(i, j)$  is the DSSIM value at the pixel position  $(i, j)$ . The variables  $x$  and  $y$  represent the local square windows centered at  $(i, j)$  in the original and manipulated images.  $\mu_x$  and  $\mu_y$  are the mean intensities of windows  $x$  and  $y$ , while  $\sigma_x$  and  $\sigma_y$  denote the variances of the corresponding windows.  $\sigma_{xy}$  represents the covariance between the two windows. The constants  $C_1$  and  $C_2$  are small values added to ensure numerical stability. Notably, DSSIM maps are computed only for the manipulated images, while real images are assigned pure black maps to represent zero dissimilarity.

**Diffusion Model Training.** We train our generative model following the Denoising Diffusion Probabilistic Model

(DDPM) framework (Ho, Jain, and Abbeel 2020), which involves two primary processes: a forward diffusion process and a reverse denoising process. The forward process is a fixed Markov chain that progressively adds Gaussian noise to a clean image  $x_0$  over  $T$  timesteps. This process has a key property that a noisy image  $x_t$  at any timestep  $t$  can be directly sampled from the original image  $x_0$  as follows:

$$x_t = \sqrt{\bar{\alpha}_t}x_0 + \sqrt{1 - \bar{\alpha}_t}\epsilon, \quad (2)$$

where  $\epsilon \sim \mathcal{N}(0, \mathbf{I})$  is a random noise sample and  $\bar{\alpha}_t$  is a parameter derived from a predefined noise schedule that dictates the noise level at timestep  $t$ . The reverse process aims to train a denoising network  $\epsilon_\theta(x_t, t)$  that predicts the noise  $\epsilon$  added to the noisy image  $x_t$ . The training objective is to minimize the Mean Squared Error (MSE) between the predicted noise and the true noise, formulated as:

$$\mathcal{L}_{\text{MSE}} = \mathbb{E}_{x_0, \epsilon, t} [\|\epsilon - \epsilon_\theta(x_t, t)\|_2^2]. \quad (3)$$

**Diffusion Model Inference.** During inference, the trained generative model reverses the forward diffusion process to reconstruct clean images from noisy inputs. Starting from a fully noisy image  $x_T$ , the model iteratively applies the reverse denoising process to recover the clean image  $x_0$ . At each timestep  $t$ , the denoising network  $\epsilon_\theta(x_t, t)$  predicts the noise  $\epsilon$  added to the image. The model then removes the predicted noise from the current noisy image  $x_t$  to produce a less noisy version  $x_{t-1}$ , using the following update rule:

$$x_{t-1} = \frac{1}{\sqrt{\bar{\alpha}_t}} (x_t - \sqrt{1 - \bar{\alpha}_t}\epsilon_\theta(x_t, t)). \quad (4)$$

This process is repeated for each  $t$  from  $T$  down to 1, gradually refining the image until a clean sample is generated.

### DiffusionFF

**Overall Architecture.** The proposed DiffusionFF framework boosts face forgery detection through Diffusion-based artifact localization, as illustrated in Figure 3. Given an input image, a pretrained forgery detector first extracts multi-resolution features that encode manipulation clues. These

features are then injected into a diffusion model via conditioning projectors to guide the generation process. Starting from pure noise, the diffusion model progressively creates a high-quality DSSIM map that reveals subtle traces of manipulation. An artifact feature extractor subsequently captures informative features from the generated DSSIM map. Finally, these artifact features are fused with high-level features from the final stage of the forgery detector through a gating mechanism to produce the classification result.

**Conditional DSSIM Map Generation via Diffusion.** In previous studies, direct regression frameworks have been employed to generate DSSIM maps. However, these methods often smooth out subtle manipulation traces, resulting in blurry and imprecise artifact localization. In contrast, diffusion models inherently support iterative refinement, allowing them to progressively enhance outputs and better capture fine-grained inconsistencies. Motivated by this advantage, we reformulate DSSIM map generation as a conditional image-to-image translation task, where a denoising diffusion model is conditioned on the input face image to synthesize high-quality DSSIM maps. To guide this generation process, we incorporate multi-resolution features extracted from a pretrained forgery detector. These features encode rich forgery-related priors that are crucial for precise artifact localization. Importantly, we find that jointly training the detector and diffusion model from scratch leads to training instability or even collapse, emphasizing the necessity of injecting pre-learned forgery knowledge into the generation pipeline. To effectively integrate these priors, we design a set of conditioning projectors that adapt the spatial and channel dimensions of the detector’s multi-resolution features to match the corresponding encoder stages of the U-Net backbone (Ronneberger, Fischer, and Brox 2015) used in the diffusion model. The transformed features are then injected into their respective U-Net stages, enabling the diffusion model to fully leverage the detector’s guidance and generate precise and fine-grained artifact localization maps.

**Feature Fusion and Classification.** Figure 2 reveals a strong correlation between the quality of DSSIM maps and detection performance, as higher-quality maps lead to more accurate results. Therefore, we leverage the generated high-fidelity DSSIM map to guide the final classification. Specifically, an artifact feature extractor first encodes the DSSIM map into artifact-aware features that capture subtle manipulation traces. These features are spatially and channel-wise aligned with the high-level semantic features extracted in the final stage of the forgery detector. The two complementary feature sets are then fused via a gating mechanism, allowing the model to selectively emphasize manipulation-relevant regions. Finally, a linear projection layer is applied to the fused representation to produce the classification outcome.

**Training Strategy.** Given the significant differences between generation and classification tasks, jointly optimizing them often leads to suboptimal performance for both. To address this challenge, we propose a two-stage training strategy that fully decouples the two tasks at the training level, enabling dedicated and specialized optimization for each. In

the first stage, we freeze the pretrained forgery detector and focus on training the conditioning projectors and the denoising diffusion model. This stage is guided by the loss function defined in Equation 3, ensuring the model is effectively optimized for the generation task. In the second stage, we freeze the forgery detector, conditioning projectors, and diffusion model, and instead optimize the artifact feature extractor alongside the classifier. This stage employs the standard Cross-Entropy (CE) loss to enhance classification performance. Our two-stage training strategy fully leverages the capabilities of each network component, ultimately maximizing the effectiveness of the DiffusionFF framework.

## Experiments

### Setup

**Datasets.** We perform training and intra-dataset evaluation on the widely used FaceForensics++ (FF++) dataset (Rossler et al. 2019), which contains 1,000 real face videos and 4,000 fake ones generated by four representative manipulation techniques: DeepFakes (DF), Face2Face (F2F) (Thies et al. 2016), FaceSwap (FS), and NeuralTextures (NT) (Thies, Zollhöfer, and Nießner 2019). For cross-dataset evaluation, we select four popular benchmarks: Celeb-DeepFake-v2 (CDF2) (Li et al. 2020), which applies advanced deepfake generation methods to YouTube celebrity videos; the DeepFake Detection Challenge (DFDC) (Dolhansky et al. 2020) and its Preview version (DFDCP) (Dolhansky et al. 2019), which contain videos with various perturbations such as compression, downsampling, and noise, leading to spatial or temporal misalignment between real and fake samples that prevents the generation of GT DSSIM maps; and FFIW-10K (FFIW) (Zhou et al. 2021), which adds complexity by incorporating multi-person scenarios.

**Baselines.** We compare our approach with sixteen SOTA baselines for face forgery detection, including ten detection-only methods: DCL (Sun et al. 2022), SBI (Shiohara and Yamasaki 2022), F<sup>2</sup>Trans (Miao et al. 2023), SeeABLE (Larue et al. 2023), LAA-Net (Nguyen et al. 2024), RAE (Tian et al. 2024), FreqBlender (Zhou et al. 2024), UDD (Fu et al. 2025), LESB (Soltandoost et al. 2025), and DFD-FCG (Han et al. 2025); and six detection with localization methods: LRL (Chen et al. 2021), PCL+I2G (Zhao et al. 2021), LiSiam (Wang, Sun, and Tang 2022), AUNet (Bai et al. 2023), Delocate (Hu et al. 2024), and KFD (Yu et al. 2025). These baselines cover comprehensive technical paradigms.

**Evaluation Metrics.** We evaluate detection performance using the Area Under the Receiver Operating Characteristic Curve (AUC), a widely used metric in face forgery detection. Video-level results are reported by averaging frame-level predictions across each video. To assess the quality of the generated DSSIM maps, we adopt four standard image quality metrics: Peak Signal-to-Noise Ratio (PSNR), Structural Similarity (SSIM) (Wang et al. 2004), Learned Perceptual Image Patch Similarity (LPIPS) (Zhang et al. 2018), and Fréchet Inception Distance (FID) (Heusel et al. 2017).

**Implementation Details.** For forgery detection, we adopt the preprocessing techniques, data augmentation strategies,

Method	Venue	Localization		Test Set AUC (%) $\uparrow$			
		Mask	DSSIM	CDF2	DFDC	DFDCP	FFIW
DCL (Sun et al.)	AAAI 2022	$\times$	$\times$	82.30	-	76.71	71.14
SBI (Shiohara and Yamasaki)	CVPR 2022	$\times$	$\times$	93.18	72.42	86.15	84.83
F <sup>2</sup> Trans (Miao et al.)	TIFS 2023	$\times$	$\times$	89.87	-	76.15	-
SeeABLE (Larue et al.)	ICCV 2023	$\times$	$\times$	87.30	75.90	86.30	-
LAA-Net (Nguyen et al.)	CVPR 2024	$\times$	$\times$	95.40	-	86.94	-
RAE (Tian et al.)	ECCV 2024	$\times$	$\times$	<u>95.50</u>	80.20	89.50	-
FreqBlender (Zhou et al.)	NeurIPS 2024	$\times$	$\times$	94.59	74.59	87.56	<u>86.14</u>
UDD (Fu et al.)	AAAI 2025	$\times$	$\times$	93.10	81.20	88.10	-
LESB (Soltandoost et al.)	WACVW 2025	$\times$	$\times$	93.13	71.98	-	83.01
DFD-FCG (Han et al.)	CVPR 2025	$\times$	$\times$	95.00	<u>81.81</u>	-	-
LRL* (Chen et al.)	AAAI 2021	$\times$	$\checkmark$	91.70	76.66	81.18	82.00
PCL+I2G (Zhao et al.)	ICCV 2021	$\checkmark$	$\times$	90.03	67.52	74.37	-
LiSiam* (Wang, Sun, and Tang)	TIFS 2022	$\times$	$\checkmark$	90.36	72.59	82.06	76.52
AUNet (Bai et al.)	CVPR 2023	$\checkmark$	$\times$	92.77	73.82	86.16	81.45
Delocate (Hu et al.)	IJCAI 2024	$\checkmark$	$\times$	91.30	-	84.00	-
KFD (Yu et al.)	ICML 2025	$\checkmark$	$\times$	94.71	79.12	<u>91.81</u>	-
DiffusionFF (Ours)	-	$\times$	$\checkmark$	<b>97.24</b>	<b>85.05</b>	<b>92.56</b>	<b>88.56</b>

Table 1: Cross-dataset face forgery detection performance on the CDF2, DFDC, DFDCP, and FFIW benchmarks. Methods marked with \* are reproduced, while results for others are directly cited from the original papers. For each dataset, the best result is highlighted in **bold** and the second-best is underlined. Methods above the horizontal divider are detection-only, while those below are detection with localization approaches. Notably, DiffusionFF achieves SOTA performance across all datasets.

Dataset	Method	Evaluation Metrics			
		PSNR $\uparrow$	SSIM $\uparrow$	LPIPS $\downarrow$	FID $\downarrow$
CDF2	LiSiam	21.985	0.367	0.464	256.201
	LRL	20.801	0.422	0.455	258.674
	DiffusionFF	<b>30.697</b>	<b>0.546</b>	<b>0.376</b>	<b>98.982</b>
FFIW	LiSiam	23.689	0.421	0.446	284.271
	LRL	23.999	0.460	0.409	248.781
	DiffusionFF	<b>32.828</b>	<b>0.529</b>	<b>0.394</b>	<b>191.798</b>

Table 2: Cross-dataset localization performance. GT DSSIM maps cannot be computed for the DFDC and DFDCP datasets because their real and fake videos are not aligned.

and testing pipeline developed by SBI (Shiohara and Yamasaki 2022). For artifact localization, we generate GT DSSIM maps on the FF++, CDF2, and FFIW datasets using the procedure outlined in the *Preliminaries* section. We employ a ConvNeXt-B network (Liu et al. 2022) pretrained on the FF++ dataset as the forgery detector, which consists of four hierarchical stages. For the denoising diffusion model, we use a standard U-Net architecture (Ronneberger, Fischer, and Brox 2015) enhanced with a timestep encoder. Our two-stage training strategy is configured as follows. In the first stage, we train the conditioning projectors and the diffusion model for 100 epochs using the AdamW optimizer, with a batch size of 96 and an initial learning rate of  $1 \times 10^{-4}$ ,

Method	Test Set AUC (%) $\uparrow$				
	DF	F2F	FS	NT	FF++
LRL	<b>100</b>	<b>100</b>	99.95	99.59	99.88
PCL+I2G	<b>100</b>	99.57	<b>100</b>	99.58	99.79
LiSiam	<b>100</b>	99.99	99.99	99.46	99.86
AUNet	<b>100</b>	99.86	99.98	99.71	99.89
RAE	99.60	99.10	99.20	97.60	98.90
DiffusionFF	<b>100</b>	<b>100</b>	99.90	<b>99.86</b>	<b>99.94</b>

Table 3: Intra-dataset detection performance on the FF++ dataset. DiffusionFF yields the best overall results.

which follows a cosine decay schedule. The total number of denoising steps is set to  $T = 50$ . In the second stage, the remaining components of the network are trained for five epochs using AdamW, with a batch size of 128 and a fixed learning rate of  $5 \times 10^{-5}$ . All experiments are implemented in the PyTorch framework and executed on a cluster of eight NVIDIA RTX 3090 GPUs. For further implementation details, please refer to the supplementary material.

## Results

**Cross-Dataset Evaluation.** Cross-dataset evaluation is a crucial protocol for assessing the generalization ability of face forgery detection models on previously unseen data. As shown in Table 1, we compare our method against recent



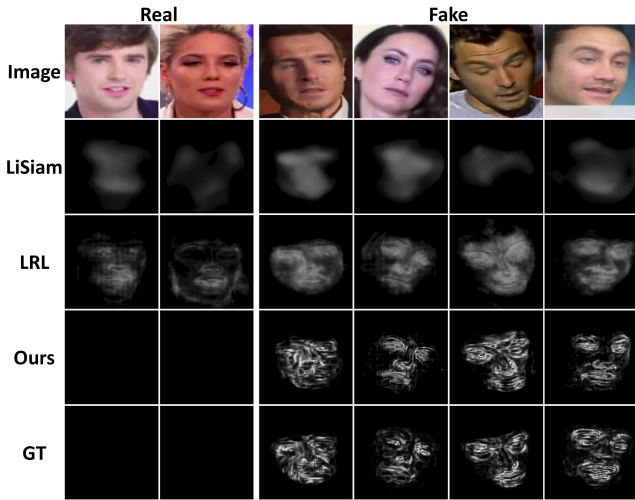


Figure 4: Qualitative artifact localization results on the CDF2 dataset. Our method generates more precise and fine-grained DSSIM maps than other DSSIM-based techniques.

Method	Evaluation Metrics			
	PSNR $\uparrow$	SSIM $\uparrow$	LPIPS $\downarrow$	FID $\downarrow$
LiSiam	20.753	0.408	0.426	292.149
LRL	23.608	0.595	0.326	241.625
DiffusionFF	<b>26.376</b>	<b>0.718</b>	<b>0.198</b>	<b>43.093</b>

Table 4: Intra-dataset localization performance on the FF++ dataset. Our method demonstrates superior performance compared to existing DSSIM-based approaches, with particularly significant improvement observed in the FID metric.

SOTA approaches for face forgery detection. The proposed DiffusionFF framework outperforms all competing models, achieving the highest AUC scores across all unseen datasets, demonstrating its exceptional generalization capability. For artifact localization, we further compare our method with existing DSSIM-based techniques. The quantitative results in Table 2 and qualitative outcomes in Figure 4 highlight the superior effectiveness of DiffusionFF. This remarkable performance can be attributed to the novel application of diffusion models, coupled with the effective integration of high-quality DSSIM maps and forgery-related semantic features.

**Intra-Dataset Evaluation.** In Table 3, we present a comparison of the intra-dataset detection performance between DiffusionFF and existing methods, showcasing the superior forgery detection capability of our approach. Furthermore, the quantitative results in Table 4 and qualitative outcomes in Figure 5 demonstrate the effectiveness of DiffusionFF in generating precise and fine-grained localization maps.

## Ablation Studies

In this section, we perform ablation studies on the diffusion model, fusion module, and forgery detector to validate the effectiveness of the proposed DiffusionFF. **Further abla-**

Method	Evaluation Metrics			
	PSNR $\uparrow$	SSIM $\uparrow$	LPIPS $\downarrow$	FID $\downarrow$
Direct Regression	24.341	0.584	0.252	172.213
Latent-Space Diffusion	24.228	0.680	0.217	56.384
Final-Stage Cond.	26.154	0.711	0.204	43.812
Decoder Cond.	26.253	0.716	0.202	46.329
The Proposed	<b>26.376</b>	<b>0.718</b>	<b>0.198</b>	<b>43.093</b>

Table 5: Ablation study results for our denoising diffusion model. The proposed method achieves the best artifact localization performance, validating the effectiveness of our design choices. “Cond.” is short for conditioning.

Method	Test Set AUC (%) $\uparrow$				Avg.
	CDF2	DFDC	DFDCP	FFIW	
Addition	95.79	84.68	91.56	88.38	90.10
Hadamard Product	96.46	84.53	91.37	88.40	90.19
Concatenation	96.66	85.00	91.87	<b>89.01</b>	90.64
Cross-Attention	97.19	84.91	92.26	88.46	90.71
Gating Mechanism	<b>97.24</b>	<b>85.05</b>	<b>92.56</b>	88.56	<b>90.85</b>

Table 6: Ablation study results for the fusion module. The gating mechanism surpasses other fusion strategies in detection performance, underscoring the efficacy of our design.

**tion experiments, including analyses of the total denoising steps, denoising seed, and two-stage training strategy, are detailed in the supplementary material.**

**Diffusion Model.** We conduct a series of ablation studies to evaluate the design choices of our denoising diffusion model for high-quality DSSIM map generation. Specifically, our experiments investigate: (1) the effectiveness of the iterative generation process versus direct regression; (2) the impact of utilizing diffusion models at the pixel level rather than in the latent space (Rombach et al. 2022); (3) the advantages of multi-stage conditioning over conditioning only at the final stage; and (4) the benefits of encoder-based conditioning compared to conditioning on the U-Net decoder. The quantitative artifact localization results, as summarized in Table 5, validate the soundness of our design decisions.

**Fusion Module.** To assess the effectiveness of the gating mechanism for feature fusion, we perform comparative experiments against several alternative strategies, including addition, Hadamard product, concatenation, and cross-attention (Dosovitskiy et al. 2021). The cross-dataset detection results, presented in Table 6, demonstrate the superior performance of the gating mechanism in seamlessly integrating artifact features with forgery-related features.

**Forgery Detector.** We conduct a comprehensive set of experiments to evaluate the impact of different forgery detectors on the proposed DiffusionFF framework. Specifically, we examine the standalone performance of two CNN-based models, EfficientNet (Shiohara and Yamasaki 2022) and

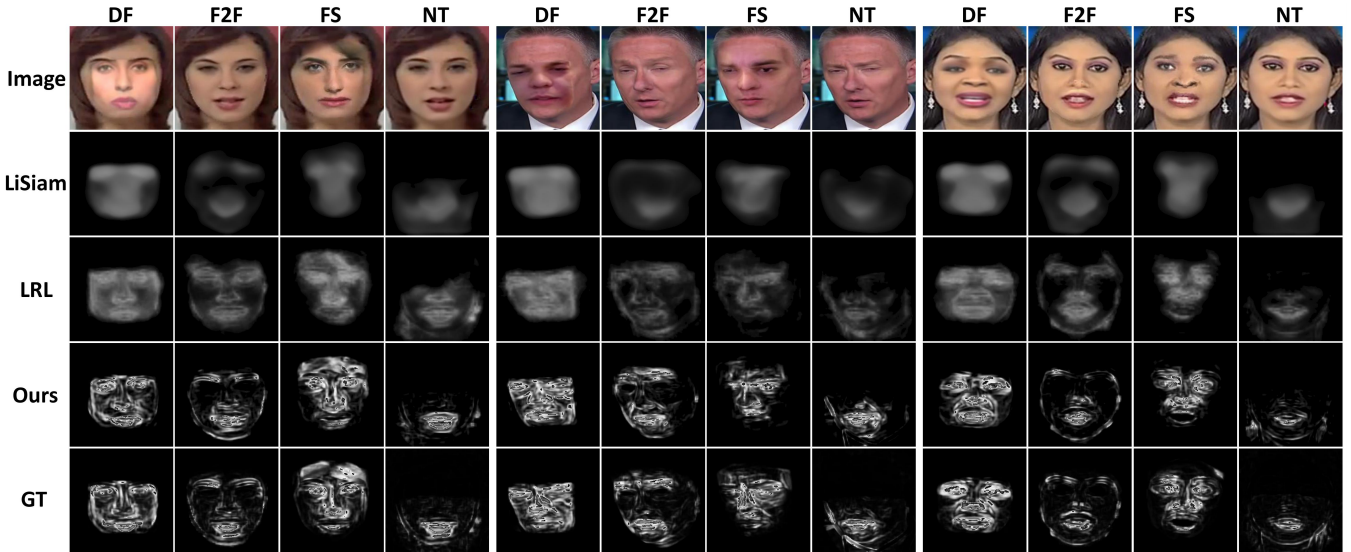


Figure 5: Qualitative results of artifact localization on the FF++ dataset.

Method	Params	Test Set AUC (%) $\uparrow$			
		CDF2	DFDC	DFDCP	FFIW
EfficientNet-B4	19M	93.18	72.42	86.15	84.83
+ DiffusionFF	32M	95.54	82.19	89.03	86.37
Swin-B	88M	95.59	82.81	89.74	85.38
+ DiffusionFF	101M	96.93	84.54	90.78	87.01
ConvNeXt-B	89M	96.08	84.26	90.20	87.67
+ DiffusionFF	102M	<b>97.24</b>	<b>85.05</b>	<b>92.56</b>	<b>88.56</b>

Table 7: Ablation study results for the forgery detector. When integrated into the DiffusionFF framework, the ConvNeXt backbone achieves the best performance among all evaluated detectors. Additionally, DiffusionFF consistently enhances the detection accuracy of each forgery detector.

ConvNeXt (Liu et al. 2022), along with the Transformer-based Swin model (Liu et al. 2021). We then assess their effectiveness when integrated into the DiffusionFF framework. The Vision Transformer (ViT) (Dosovitskiy et al. 2021) is excluded from our study due to its single-scale feature representation, which is fundamentally incompatible with DiffusionFF’s multi-stage conditioning mechanism. As shown in Table 7, all detectors exhibit consistent and substantial improvements in cross-dataset detection performance when augmented with DiffusionFF. Additionally, t-SNE visualizations in Figure 6 further illustrate that DiffusionFF facilitates a more distinct separation between real and fake samples than using the detector alone. These results demonstrate that the high-quality DSSIM maps generated by DiffusionFF can significantly boost detection accuracy, establishing it as a robust, explainable, and plug-and-play enhancement for existing face forgery detection models.

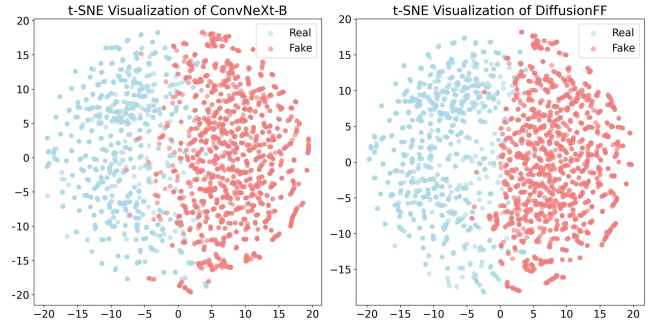


Figure 6: t-SNE visualizations of feature representations extracted by ConvNeXt and the proposed DiffusionFF on the CDF2 dataset. DiffusionFF produces more distinct and well-separated clusters, demonstrating its enhanced discriminative capability over the standalone ConvNeXt.

## Conclusion

In this paper, we propose DiffusionFF, a novel framework that enhances face forgery detection through Diffusion-based artifact localization. Our primary contributions are as follows. First, we pioneer the application of denoising diffusion models to generate high-quality DSSIM maps that effectively capture subtle manipulation traces. Second, we seamlessly integrate these DSSIM maps with high-level semantic features extracted by a forgery detector, significantly improving classification accuracy. The proposed DiffusionFF not only achieves SOTA performance in face forgery detection but also delivers precise and fine-grained localization of manipulation artifacts. Comprehensive ablation studies underscore the effectiveness of our design, establishing DiffusionFF as a robust, explainable, and easily integrable enhancement for existing forgery detectors.

## References

- Bai, W.; Liu, Y.; Zhang, Z.; Li, B.; and Hu, W. 2023. AUNet: Learning Relations Between Action Units for Face Forgery Detection. In *Proceedings of the IEEE/CVF Conference on Computer Vision and Pattern Recognition (CVPR)*, 24709–24719.
- Buslaev, A.; Iglovikov, V. I.; Khvedchenya, E.; Parinov, A.; Druzhinin, M.; and Kalinin, A. A. 2020. Albumentations: fast and flexible image augmentations. *Information*, 11(2): 125.
- Chen, S.; Yao, T.; Chen, Y.; Ding, S.; Li, J.; and Ji, R. 2021. Local relation learning for face forgery detection. In *Proceedings of the AAAI conference on artificial intelligence (AAAI)*, volume 35, 1081–1088.
- Chen, S.; Yao, T.; Liu, H.; Sun, X.; Ding, S.; Ji, R.; et al. 2024. Diffusionfake: Enhancing generalization in deepfake detection via guided stable diffusion. *Advances in Neural Information Processing Systems (NeurIPS)*, 37: 101474–101497.
- Cui, X.; Li, Y.; Luo, A.; Zhou, J.; and Dong, J. 2025. Forensics adapter: Adapting clip for generalizable face forgery detection. In *Proceedings of the Computer Vision and Pattern Recognition Conference (CVPR)*, 19207–19217.
- Deng, J.; Guo, J.; Ververas, E.; Kotsia, I.; and Zafeiriou, S. 2020. RetinaFace: Single-Shot Multi-Level Face Localisation in the Wild. In *Proceedings of the IEEE/CVF Conference on Computer Vision and Pattern Recognition (CVPR)*.
- Dolhansky, B.; Bitton, J.; Pflaum, B.; Lu, J.; Howes, R.; Wang, M.; and Ferrer, C. C. 2020. The deepfake detection challenge (dfdc) dataset. *arXiv preprint arXiv:2006.07397*.
- Dolhansky, B.; Howes, R.; Pflaum, B.; Baram, N.; and Ferrer, C. C. 2019. The deepfake detection challenge (dfdc) preview dataset. *arXiv preprint arXiv:1910.08854*.
- Dosovitskiy, A.; Beyer, L.; Kolesnikov, A.; Weissenborn, D.; Zhai, X.; Unterthiner, T.; Dehghani, M.; Minderer, M.; Heigold, G.; Gelly, S.; Uszkoreit, J.; and Housley, N. 2021. An Image is Worth 16x16 Words: Transformers for Image Recognition at Scale. In *International Conference on Learning Representation (ICLR)*.
- Fu, X.; Yan, Z.; Yao, T.; Chen, S.; and Li, X. 2025. Exploring unbiased deepfake detection via token-level shuffling and mixing. In *Proceedings of the AAAI Conference on Artificial Intelligence (AAAI)*, volume 39, 3040–3048.
- Guo, X.; Liu, X.; Ren, Z.; Grosz, S.; Masi, I.; and Liu, X. 2023. Hierarchical Fine-Grained Image Forgery Detection and Localization. In *Proceedings of the IEEE/CVF Conference on Computer Vision and Pattern Recognition (CVPR)*, 3155–3165.
- Han, Y.-H.; Huang, T.-M.; Hua, K.-L.; and Chen, J.-C. 2025. Towards More General Video-based Deepfake Detection through Facial Component Guided Adaptation for Foundation Model. In *Proceedings of the IEEE/CVF Conference on Computer Vision and Pattern Recognition (CVPR)*, 22995–23005.
- He, P.; Li, H.; and Wang, H. 2019. Detection of Fake Images Via The Ensemble of Deep Representations from Multi Color Spaces. In *2019 IEEE International Conference on Image Processing (ICIP)*, 2299–2303.
- Heusel, M.; Ramsauer, H.; Unterthiner, T.; Nessler, B.; and Hochreiter, S. 2017. Gans trained by a two time-scale update rule converge to a local nash equilibrium. *Advances in neural information processing systems (NeurIPS)*, 30.
- Ho, J.; Jain, A.; and Abbeel, P. 2020. Denoising diffusion probabilistic models. *Advances in neural information processing systems (NeurIPS)*, 33: 6840–6851.
- Hsu, G.-S.; Tsai, C.-H.; and Wu, H.-Y. 2022. Dual-Generator Face Reenactment. In *Proceedings of the IEEE/CVF Conference on Computer Vision and Pattern Recognition (CVPR)*, 642–650.
- Hu, J.; Liao, X.; Gao, D.; Tsutsui, S.; Wang, Q.; Qin, Z.; and Shou, M. Z. 2024. Delocate: detection and localization for deepfake videos with randomly-located tampered traces. In *Proceedings of the Thirty-Third International Joint Conference on Artificial Intelligence (IJCAI)*.
- Kong, C.; Chen, B.; Li, H.; Wang, S.; Rocha, A.; and Kwong, S. 2022. Detect and locate: Exposing face manipulation by semantic-and noise-level telltales. *IEEE Transactions on Information Forensics and Security*, 17: 1741–1756.
- Larue, N.; Vu, N.-S.; Struc, V.; Peer, P.; and Christophides, V. 2023. SeeABLE: Soft Discrepancies and Bounded Contrastive Learning for Exposing Deepfakes. In *Proceedings of the IEEE/CVF International Conference on Computer Vision (ICCV)*, 21011–21021.
- Li, J.; Xie, H.; Yu, L.; and Zhang, Y. 2022. Wavelet-enhanced Weakly Supervised Local Feature Learning for Face Forgery Detection. In *Proceedings of the 30th ACM International Conference on Multimedia (ACM MM)*, 1299–1308.
- Li, Y.; Yang, X.; Sun, P.; Qi, H.; and Lyu, S. 2020. Celeb-DF: A Large-Scale Challenging Dataset for Deep-Fake Forensics. In *Proceedings of the IEEE/CVF Conference on Computer Vision and Pattern Recognition (CVPR)*.
- Liu, Z.; Lin, Y.; Cao, Y.; Hu, H.; Wei, Y.; Zhang, Z.; Lin, S.; and Guo, B. 2021. Swin Transformer: Hierarchical Vision Transformer Using Shifted Windows. In *Proceedings of the IEEE/CVF International Conference on Computer Vision (ICCV)*, 10012–10022.
- Liu, Z.; Mao, H.; Wu, C.-Y.; Feichtenhofer, C.; Darrell, T.; and Xie, S. 2022. A ConvNet for the 2020s. In *Proceedings of the IEEE/CVF Conference on Computer Vision and Pattern Recognition (CVPR)*, 11976–11986.
- McCloskey, S.; and Albright, M. 2019. Detecting GAN-Generated Imagery Using Saturation Cues. In *2019 IEEE International Conference on Image Processing (ICIP)*, 4584–4588.
- Miao, C.; Tan, Z.; Chu, Q.; Liu, H.; Hu, H.; and Yu, N. 2023. F2Trans: High-Frequency Fine-Grained Transformer for Face Forgery Detection. *IEEE Transactions on Information Forensics and Security*, 18: 1039–1051.
- Nguyen, D.; Mejri, N.; Singh, I. P.; Kuleshova, P.; Astrid, M.; Kacem, A.; Ghorbel, E.; and Aouada, D. 2024. LAA-Net: Localized Artifact Attention Network for Quality-



- Agnostic and Generalizable Deepfake Detection. In *Proceedings of the IEEE/CVF Conference on Computer Vision and Pattern Recognition (CVPR)*, 17395–17405.
- Qian, Y.; Yin, G.; Sheng, L.; Chen, Z.; and Shao, J. 2020. Thinking in frequency: Face forgery detection by mining frequency-aware clues. In *Proceedings of The 16th European conference on computer vision (ECCV)*, 86–103. Springer.
- Rombach, R.; Blattmann, A.; Lorenz, D.; Esser, P.; and Ommer, B. 2022. High-resolution image synthesis with latent diffusion models. In *Proceedings of the IEEE/CVF conference on computer vision and pattern recognition (CVPR)*, 10684–10695.
- Ronneberger, O.; Fischer, P.; and Brox, T. 2015. U-net: Convolutional networks for biomedical image segmentation. In *International Conference on Medical Image Computing and Computer Assisted Intervention (MICCAI)*, 234–241. Springer.
- Rossler, A.; Cozzolino, D.; Verdoliva, L.; Riess, C.; Thies, J.; and Niessner, M. 2019. FaceForensics++: Learning to Detect Manipulated Facial Images. In *Proceedings of the IEEE/CVF International Conference on Computer Vision (ICCV)*.
- Shiohara, K.; and Yamasaki, T. 2022. Detecting Deepfakes With Self-Blended Images. In *Proceedings of the IEEE/CVF Conference on Computer Vision and Pattern Recognition (CVPR)*, 18720–18729.
- Shiohara, K.; Yang, X.; and Taketomi, T. 2023. Blend-Face: Re-designing Identity Encoders for Face-Swapping. In *Proceedings of the IEEE/CVF International Conference on Computer Vision (ICCV)*, 7634–7644.
- Soltandoost, E.; Plesh, R.; Schuckers, S.; Peer, P.; and Štruc, V. 2025. Extracting Local Information from Global Representations for Interpretable Deepfake Detection. In *Proceedings of the Winter Conference on Applications of Computer Vision (WACV) Workshops*, 1629–1639.
- Sun, K.; Yao, T.; Chen, S.; Ding, S.; Li, J.; and Ji, R. 2022. Dual contrastive learning for general face forgery detection. In *Proceedings of the AAAI Conference on Artificial Intelligence (AAAI)*, volume 36, 2316–2324.
- Tan, C.; Zhao, Y.; Wei, S.; Gu, G.; Liu, P.; and Wei, Y. 2024. Frequency-aware deepfake detection: Improving generalizability through frequency space domain learning. In *Proceedings of the AAAI Conference on Artificial Intelligence (AAAI)*, volume 38, 5052–5060.
- Thies, J.; Zollhöfer, M.; and Nießner, M. 2019. Deferred neural rendering: Image synthesis using neural textures. *ACM Transactions on Graphics*, 38(4): 1–12.
- Thies, J.; Zollhofer, M.; Stamminger, M.; Theobalt, C.; and Niessner, M. 2016. Face2Face: Real-Time Face Capture and Reenactment of RGB Videos. In *Proceedings of the IEEE Conference on Computer Vision and Pattern Recognition (CVPR)*.
- Tian, J.; Yu, C.; Wang, X.; Chen, P.; Xiao, Z.; Dai, J.; Han, J.; and Chai, Y. 2024. Real Appearance Modeling for More General Deepfake Detection. In *Proceedings of The 18th European Conference on Computer Vision (ECCV)*, 402–419.
- Wang, J.; Sun, Y.; and Tang, J. 2022. LiSiam: Localization invariance Siamese network for deepfake detection. *IEEE Transactions on Information Forensics and Security*, 17: 2425–2436.
- Wang, Z.; Bovik, A.; Sheikh, H.; and Simoncelli, E. 2004. Image quality assessment: from error visibility to structural similarity. *IEEE Transactions on Image Processing*, 13(4): 600–612.
- Yan, Z.; Luo, Y.; Lyu, S.; Liu, Q.; and Wu, B. 2024. Transcending Forgery Specificity with Latent Space Augmentation for Generalizable Deepfake Detection. In *Proceedings of the IEEE/CVF Conference on Computer Vision and Pattern Recognition (CVPR)*, 8984–8994.
- Yang, Z.; Liang, J.; Xu, Y.; Zhang, X.-Y.; and He, R. 2023. Masked Relation Learning for DeepFake Detection. *IEEE Transactions on Information Forensics and Security*, 18: 1696–1708.
- Yu, P.; Fei, J.; Gao, H.; Feng, X.; Xia, Z.; and Chang, C. H. 2025. Unlocking the capabilities of vision-language models for generalizable and explainable deepfake detection. *arXiv e-prints*, arXiv–2503.
- Yu, Z.; Ni, J.; Lin, Y.; Deng, H.; and Li, B. 2024. Difforensics: Leveraging diffusion prior to image forgery detection and localization. In *Proceedings of the IEEE/CVF Conference on Computer Vision and Pattern Recognition (CVPR)*, 12765–12774.
- Zhang, D.; Xiao, Z.; Li, S.; Lin, F.; Li, J.; and Ge, S. 2024. Learning natural consistency representation for face forgery video detection. In *Proceedings of The 18th European Conference on Computer Vision (ECCV)*, 407–424. Springer.
- Zhang, L.; Rao, A.; and Agrawala, M. 2023. Adding conditional control to text-to-image diffusion models. In *Proceedings of the IEEE/CVF international conference on computer vision (CVPR)*, 3836–3847.
- Zhang, R.; Isola, P.; Efros, A. A.; Shechtman, E.; and Wang, O. 2018. The Unreasonable Effectiveness of Deep Features as a Perceptual Metric. In *Proceedings of the IEEE Conference on Computer Vision and Pattern Recognition (CVPR)*.
- Zhao, H.; Liu, B.; Hu, Y.; Li, J.; and Li, C.-T. 2023. Hybrid domain meta-learning network for face forgery detection and localization in deepfakes. In *2023 International Joint Conference on Neural Networks (IJCNN)*, 1–8. IEEE.
- Zhao, T.; Xu, X.; Xu, M.; Ding, H.; Xiong, Y.; and Xia, W. 2021. Learning Self-Consistency for Deepfake Detection. In *Proceedings of the IEEE/CVF International Conference on Computer Vision (ICCV)*, 15023–15033.
- Zhou, J.; Li, Y.; Wu, B.; Li, B.; Dong, J.; et al. 2024. Fre-qBlender: Enhancing DeepFake Detection by Blending Frequency Knowledge. In *Advances in Neural Information Processing Systems (NeurIPS)*, volume 37, 44965–44988.
- Zhou, T.; Wang, W.; Liang, Z.; and Shen, J. 2021. Face Forensics in the Wild. In *Proceedings of the IEEE/CVF Conference on Computer Vision and Pattern Recognition (CVPR)*, 5778–5788.

## Supplementary Material

### Implementation Details

**SBI.** The SBI framework (Shiohara and Yamasaki 2022) generates synthetic face images from real samples by simulating the deepfake generation pipeline. It comprises two key components: the Source-Target Generator (STG) and the Mask Generator (MG). The STG applies a series of image transformations to produce pseudo-source and pseudo-target images, while the MG creates a blending mask using pre-detected facial landmarks, with augmentation to enhance diversity. These pseudo-source and pseudo-target images are then combined using the blending mask to produce a pseudo-fake face. In this study, we leverage the SBI framework to enrich the training data by mixing SBI-generated images with samples from the FF++ dataset (Rossler et al. 2019). Notably, the pseudo-fake images are perfectly aligned with their corresponding real counterparts, enabling the accurate generation of GT DSSIM maps.

**Preprocessing.** Facial landmarks are accurately extracted using Dlib’s 81-point predictor, which is utilized only during the training phase. For face detection, RetinaFace (Deng et al. 2020) is employed to generate facial bounding boxes. During training, each detected face is cropped with a random margin ranging from 4% to 20%, while a fixed margin of 12.5% is applied during the inference phase.

**Data Augmentation.** The image processing toolbox introduced in (Buslaev et al. 2020) is utilized for data augmentation. Within the STG module of the SBI framework, transformations including RGBShift, HueSaturationValue, RandomBrightnessContrast, Downscale, and Sharpen are applied to generate pseudo source and target images. Additionally, during training, all samples are augmented using operations such as ImageCompression, RGBShift, HueSaturationValue, and RandomBrightnessContrast.

**Other Details.** During training, we extract 32 frames from each real video and eight frames from each fake video to ensure a balanced ratio of positive and negative samples. Additionally, we select eight frames from each real video to generate corresponding pseudo-fake samples using the SBI framework, which are then integrated into the training dataset to enhance its richness. During testing, we uniformly sample 32 frames per video. For frames with multiple detected faces, we apply the classification model to each face and adopt the highest forgery score as the frame’s predicted confidence. For the diffusion model, we adopt a seven-stage U-Net with channel dimensions configured as [64, 64, 128, 256, 128, 64, 64]. The model is trained using a linear noise schedule, with beta values incrementally increasing from 0.02 to 0.4 throughout the training process. The GT DSSIM maps are generated using a local square window of size  $7 \times 7$ .

### Experimental Results

**Denosing Steps.** We investigate the impact of different denosing step counts  $T$  on the performance of the diffusion model. As shown in Table 8, the quantitative evaluation results support our choice of  $T = 50$  as a balanced trade-off between quality and efficiency. Although  $T = 100$  yields

$T$	Evaluation Metrics			
	PSNR $\uparrow$	SSIM $\uparrow$	LPIPS $\downarrow$	FID $\downarrow$
40	26.253	0.715	0.202	46.329
50	<b>26.376</b>	<b>0.718</b>	0.198	43.093
75	26.163	0.716	0.199	42.960
100	25.941	0.713	<b>0.193</b>	<b>40.363</b>

Table 8: Ablation study results for the denosing steps  $T$ .

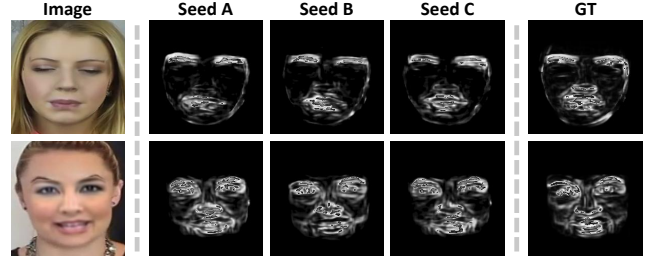


Figure 7: Effect of seed variation on generation results.

better LPIPS and FID scores, it leads to lower PSNR and SSIM values while nearly doubling the computational cost. Notably, the diffusion model fails to converge when  $T \leq 30$ .

**Denosing Seed.** We assess the effect of random seed variation on DSSIM map generation. As illustrated in Figure 7, our method produces reliable results across different seeds.

**Training Strategy.** We compare our two-stage training strategy with single-stage training. As shown in Table 9, our method yields significantly better results, highlighting the effectiveness of decoupling the generation and classification tasks during training.

### Discussions

**Using GT DSSIM Maps as Inputs During Training.** In Figure 2 of the main text, we show that higher-quality DSSIM maps contribute to more accurate predictions. This naturally raises a question: what if GT DSSIM maps are used as inputs to the artifact feature extractor during the second training stage? To investigate this, we conduct an experiment using GT maps and obtain a 96.72% AUC on the CDF2 dataset, which is lower than the 97.24% achieved with diffusion-generated maps. This performance drop is primarily due to a mismatch in value distributions: GT DSSIM maps (e.g., all zeros for real samples) differ significantly from those produced by the diffusion model. As a result, the model trained with GT DSSIM maps struggles to generalize when faced with diffusion-generated inputs during inference, ultimately leading to degraded performance.

**Comparison Between ControlNet and Our Method.** ControlNet (Zhang, Rao, and Agrawala 2023) is a widely applied framework for conditional image generation, integrating a conditioning network to guide a pretrained, frozen Stable Diffusion model (Rombach et al. 2022). In our research, we attempted to train a ControlNet for generat-

Method	Test Set AUC (%) $\uparrow$			
	CDF2	DFDC	DFDCP	FFIW
Single-Stage	95.47	83.54	90.27	87.69
Two-Stage	<b>97.24</b>	<b>85.05</b>	<b>92.56</b>	<b>88.56</b>

Table 9: Ablation study results for the training strategy.

ing DSSIM maps but encountered training collapse. We attribute this failure to a fundamental domain mismatch: the pretrained Stable Diffusion model, optimized for natural RGB images, struggles to adapt to single-channel, grayscale DSSIM maps due to its strong prior knowledge. To address this issue, we propose an inverted strategy that contrasts with the standard ControlNet approach. Instead of training a conditioning network, we employ a pretrained forgery detector as a fixed conditioning model, capitalizing on its ability to detect manipulation artifacts. By freezing this conditioning network and training the diffusion model, we shift the learning focus to the generative model itself. This reversal enables the diffusion model to effectively learn from the forgery detector’s specialized features, facilitating the successful generation of DSSIM maps.